Journal of Materials Chemistry B

ROYAL SOCIETY OF CHEMISTRY

PAPER

View Article Online
View Journal | View Issue

Check for updates

Cite this: J. Mater. Chem. B, 2022, 10, 8282

The amount of dextran in PLGA nanocarriers modulates protein corona and promotes cell membrane damage†

Luana Corsi Antonio, [a] Laís Ribovski, ‡*[ab] Paula Maria Pincela Lins §[a] and Valtencir Zucolotto [a]

Polymeric nanocarriers (NCs) are efficient vehicles to prevent drug unspecific biodistribution and increase the drug amounts delivered to tumor tissues. However, some toxicological aspects of NCs still lack a comprehensive assessment, such as their effects on cellular processes that lead to toxicity. We evaluate the interaction of poly(lactic-*co*-glycolic acid) (PLGA) NCs prepared using dextran (Dex) and Pluronic®-F127 as stabilizing agents with myocardial cells (H9C2), breast adenocarcinoma cells (MCF-7) and macrophages (RAW 264.7) to address the effect of Dex in PLGA NC formulations. By an emulsion diffusion method, doxorubicin-loaded NCs were prepared with no Dex (PLGA-DOX), 1% (w/v) Dex (Dex1/PLGA-DOX) and 5% (w/v) Dex (Dex5/PLGA-DOX). Uptake analyses revealed a significant reduction in Dex5/PLGA-DOX NC uptake by H9C2 and MCF-7, as in the case of Dex1/PLGA-DOX NCs in the absence of *in vitro* protein corona, revealing an effect of dextran concentration on the formation of protein corona. RAW 264.7 cells presented a greater uptake of Dex5/PLGA-DOX NCs than the other NCs likely because of receptor mediated endocytosis, since C-type lectins like SIGN-R1, mannose receptors and scavenger receptor type 1 that are expressed in RAW 264.7 can mediate Dex uptake. Despite the lower uptake, Dex5/PLGA-DOX NCs promote the generation of reactive oxygen species and oxidative membrane damage in MCF-7 and H9C2 even though cellular metabolic activity assessed by MTT was comparable among all the NCs. Our results highlight the importance of an in-depth investigation of the NC–cell interaction considering additional mechanisms of damage apart from metabolic variations, as nanoparticle-induced damage is not limited to imbalance in metabolic processes, but also associated with other mechanisms, *e.g.*, membrane and DNA damage.

Received 21st June 2022,
Accepted 31st August 2022

DOI: 10.1039/d2tb01296k

rsc.li/materials-b

Open Access Article. Published on 01 September 2022. Downloaded on 12/29/2025 6:58:32 AM.
This article is licensed under a Creative Commons Attribution 3.0 Unported Licence.

Introduction

The anti-cancer activity of doxorubicin (DOX) is widely known within the scientific community; however, its non-specific distribution in biological systems has limited its application.[1] In high doses, DOX can cause irreversible cardiomyopathy and even heart failure due to oxidative stress caused by increased production of reactive oxygen species (ROS).[2] Polymeric nanocarriers (NCs) are efficient vehicles to prevent DOX unspecific biodistribution and to reduce long-term adverse effects.[2,3] Poly(lactic-*co*-glycolic acid) (PLGA) is a co-polymer widely used in biomedical applications because of its biocompatibility and biodegradability; besides, it is FDA-approved. Several chemotherapeutics have been encapsulated in PLGA-based NCs and evaluated for the treatment of various types of cancers.[3,4] However, some toxicological aspects of PLGA-based formulations still lack comprehensive studies on their effects on cellular processes that can lead to cell damage and death.

In the body, the biodistribution of the NCs is affected by the adsorption of proteins on the NCs' surface, known as protein corona.[5] Some of these proteins, the opsonins, can initiate an immune response exposing the NCs to phagocytes, *e.g.*, macrophages, reducing the NCs' blood half-life.[5] Macrophages are

[a] University of São Paulo, Physics Institute of São Carlos, Nanomedicine and Nanotoxicology Group, CP 369, 13566-590, São Carlos, SP, Brazil
[b] University of Groningen, University Medical Center Groningen, Department of Biomedical Engineering, Antonius Deusinglaan 1, 9713, AV, Groningen, The Netherlands. E-mail: l.ribovski@umcg.nl

† Electronic supplementary information (ESI) available: Characterization of the NCs by Fourier transform infrared spectroscopy (FTIR); DOX calibration curve in H_2O; cell viability after 24 hours of incubation with NCs; gate strategy for *in vitro* cellular uptake studies; NC uptake by RAW 264.7 after 4 h of incubation and inhibition studies; and gate strategy for *in vitro* annexin V binding assay. See DOI: https://doi.org/10.1039/d2tb01296k

‡ The University of Groningen is this author's current address and primary affiliation.

§ P. M. P. Lins current address: Biomedical Research Institute (BIOMED), Faculty of Medicine and Life Sciences, Hasselt University, Agoralaan, 3590 Diepenbeek, Belgium.

This journal is © The Royal Society of Chemistry 2022

Open Access Article. Published on 01 September 2022. Downloaded on 12/29/2025 6:58:32 AM.
This article is licensed under a Creative Commons Attribution 3.0 Unported Licence.

also an important component of tumor progression and tissue repair.[6,7] Protein corona formation can mask surface functionalization of the NCs, leading to NCs' accumulation in the liver and spleen instead of the target sites.[8,9] The amount and composition of the adsorbed proteins vary with the surface characteristics of the NCs, *e.g.*, surface charge and surface chemistry, which impact the biological identity of the NCs.[10–12] Polyethylene glycol (PEG) coating is commonly used to provide a steric barrier to the surface of NCs reducing the opsonization and increasing the retention of the NCs in the blood.[13] However, PEGylation leads to poor NC uptake by cells into tumor tissues, suggesting that PEG coatings may not always be the optimal choice for targeted drug delivery.[13,14]

Another strategy applied to increase the circulation time of nanomaterials is the use dextran (Dex) as the coating agent due to its hydrophilicity and branched structure that reduce plasma protein adsorption.[15–17] The dextran coat can also trigger efficiently and selectively NC uptake by scavenger receptors and dextran-binding C-type lectins. Dextran-based NCs have shown enhanced tumor penetration as well as enzymatic hydrolysis through alpha amylase which is overexpressed in tumor cells.[18–21]

Iron-oxide based NCs coated with dextran showed neurotoxicity and genotoxicity due to oxidative stress.[22,23] ROS imbalance is one of the frequently reported causes of NC-associated toxicity that can promote DNA and cell membrane ROS-mediated damage.[23–25] Oxidative stress induced by NCs is dependent on particle properties, *e.g.*, surface chemistry, size and composition.[26] In-depth investigation of the NC–cell interaction is fundamental to ensure the safety of the NCs even as apparently non-toxic formulations, since effects including DNA damage, oxidative stress, and mitochondrial dysfunction can occur without detectable changes in cytotoxicity assessed by conventional colorimetric assays.[27]

We studied DOX loaded PLGA NCs prepared with 5 and 1% (w/v) or without Dex as a stabilizing and capping agent. The uptake of PLGA NCs was evaluated in the presence and absence of serum by flow cytometry. Also, membrane damage, metabolic imbalance and ROS induction were assessed to study whether Dex content affects NC interaction with breast cancer cells (MCF-7), myocardial cells (H9C2) and macrophages (RAW 264.7).

Experimental

Materials

Poly(lactide-*co*-glycolide) (PLGA) (Resomer 503H 50 : 50 M_W 24 000–38 000, acid terminated, #719870), Pluronic®-F127 (#P2443), Dextran 40 (M_r ~ 40 kDa, #31389), ethyl acetate (#319902), doxorubicin hydrochloride (#D2975000), deuterium oxide (#151882), tetrazolium blue thiazolyl bromide (MTT, #M2128), 2′-7′-dichlorodihydrofluorescein diacetate (CM-H2D CFDA, #D6883), ammonium persulfate (APS, #A3678), sodium dodecyl sulfate (SDS, #L3771), tetramethyl ethylenediamine (TEMED, #T9281), glycine, 2-mercaptoethanol (2-ME, #M6250), glycerol (#G9012), bromophenol blue (#114391), KCl (#C2010.0.AH), NaCl (#C1060.01.AH), KH_2PO_4 (#P9791) and Na_2HPO_4 (#S5136) were obtained from Sigma-Aldrich. Trypan Blue Stain (0.4% (w/v)) for use with the Countess™ Automated Cell Counter was purchased from Invitrogen™. Dimethyl sulfoxide (DMSO, #D1011.01.BJ) was obtained from Synth. Dulbecco's modified Eagle's medium (DMEM) culture media with (#00074) and without phenol, 0.25% trypsin-EDTA solution (#T2500), fetal bovine serum (FBS, #S0011) and L-glutamine 200 mmol mL^{-1} (#G0209) were obtained from Vitrocell. The FITC Annexin V Apoptosis Detection Kit I (#556547) was obtained from BD Pharmingen™. The Pierce™ BCA Protein Assay Kit (#23225) and GelCode™ Blue Stain Reagent (#24590) were obtained from Thermo Scientific™. 30% Acrylamide/BIS solution (#161-0156) was obtained from Bio-Rad Laboratories.

Syntheses of the PLGA-DOX, Dex1/PLGA-DOX and Dex5/PLGA NCs

The nanocarriers were prepared by the emulsion diffusion method.[28] 200 μL of 10 mg mL^{-1} aqueous doxorubicin solution was emulsified in 2.5 mL of ethyl acetate containing 2.5% (w/v) 50 : 50 PLGA and 5 mL of a 2.5% (w/v) aqueous solution of Pluronic®-F127. The emulsion was prepared on an ice bath by sonication in a Delta Ultrasound sonicator, model Sonifier 450D, with power equal to 550 W and 20% amplitude for 90 s. To the resulting emulsion was added 5 mL of 0.01 M phosphate buffer pH 8.6 containing 2.5% (w/v) Pluronic®-F127 and kept under moderate stirring for 1 h. Ethyl acetate was removed by evaporation under low pressure in a desiccator. For the synthesis of blank NCs, 200 μL of Milli-Q water (resistivity 18.2 MΩ cm) was sonicated with the organic phase and the surfactant solution for the formation of the first emulsion. The synthesis of the NCs in the presence of Dex was carried out by the same procedure; however, the ethyl acetate containing 2.5% (w/v) 50 : 50 PLGA was emulsified with 5 mL of Milli-Q water containing 2.5% (w/v) Pluronic®-F127 and 1 or 5% (w/v) dextran. Pluronic®-F127-stabilized NCs were also synthesized (without Dex).

Characterization of the PLGA-DOX, Dex1/PLGA-DOX and Dex5/PLGA NCs

Zeta potential and size distribution (DLS) of all the nanoparticles (NPs) were measured using Zetasizer Nano ZS, Malvern. The concentrations of the NCs were evaluated by nanotracking analysis (NTA; Nanosight NS300, Malvern), besides size assessment. NTA was performed with 50–100 particles/frame and at a camera level of 12 (shutter: 1200; gain: 146). Each formulation was diluted 10 times (10 NCs per ml) and 1000 times prior to DLS and NTA analyses, respectively.

Infrared analyses were performed using an infrared spectrometer (Nicolet 6700/GRAMS Suite), with 128 scans per sample with 4 cm^{-1} resolution from 4000 to 400 cm^{-1}. The samples were prepared by drop-casting 20 μL of the formulations in silicon wafer and dried under a reduced atmosphere. UV-visible spectra were obtained using a Hitachi U-2900 spectrophotometer, in a quartz cuvette (10 mm path length). Fluorescence spectroscopy was performed using the SpectraMax M3

Open Access Article. Published on 01 September 2022. Downloaded on 12/29/2025 6:58:32 AM. This article is licensed under a Creative Commons Attribution 3.0 Unported Licence.

Multi-Mode Microplate (Molecular Devices) controlled by SoftMax Pro software, in a four-sided polished quartz cuvette (10 mm path length).

Transmission electron microscopy (TEM) images were obtained using a JEM-2100 transmission electron microscope. 3 or 10 μL of the samples at a concentration of 10^{11} NCs per ml was deposited on copper grids for 60 s and dried with filter paper. The samples were stained with 3 μL of 2% uranyl acetate for 30 s and again dried with filter paper. Staining followed by the drying step with filter paper was repeated one more time. TEM images were analyzed using Fiji (ImageJ) to measure the diameter of 50 NCs per sample.

Proton nuclear magnetic resonance (^{1}H NMR) spectra were recorded on an Agilent technologies 400/54 Premium Shielded NMR Magnet at 400 MHz. Approximately 1.5 mg of freeze-dried Dex5/PLGA-DOX, Dex1/PLGA-DOX, and PLGA-DOX NCs was diluted with 600 μL of D_2O and transferred to a 5 mm NMR tube. The peak area ratio of (1 → 6)-α-D-glucose monomers of dextran (δ 4.98 ppm) and methyl groups of the lactic acid (δ 1.2 ppm) of PLGA estimates the dextran content in the NCs.

$$\frac{M_{\alpha\text{-D-glucose}}}{M_{\text{PLA}}} = \frac{N_{\alpha\text{-D-glucose}}}{N_{\text{PLA}}} \cdot \frac{A_{\alpha\text{-D-glucose}}}{A_{\text{PLA}}} \quad (1)$$

where A is the peak area and N is the number of nuclei giving rise to the signal.

Encapsulation efficiency (EE) and cumulative release of DOX

Doxorubicin encapsulation efficiency was determined by quantifying the samples' absorbance using UV-visible spectroscopy. 1 mL of each nanocarrier formulation – PLGA-DOX, Dex1/PLGA-DOX and Dex5/PLGA-DOX NCs – was centrifuged (10 000 g, 30 min, 20 °C) and the pellets containing the NCs were resuspended in Milli-Q water. Absorbance was measured before and after centrifugation. The encapsulation efficiency values were obtained according to eqn (2):

$$\%\text{EE} = \frac{\text{ABS}_{\text{max after centrifugation}}}{\text{ABS}_{\text{max before centrifugation}}} \quad (2)$$

To obtain the release profile of PLGA-DOX, Dex1/PLGA-DOX and Dex5/PLGA-DOX NCs, 250 μL of each formulation was centrifuged (10 000 g, 20 min, 20 °C) and resuspended in 1.5 mL of 1× PBS buffer, pH 7.4. The samples were incubated in a microtube shaker with constant agitation, at 37 °C and under protection from light.

At defined times, the samples were centrifuged (10 000 g, 20 min, 20 °C) and the supernatants collected. The pellets were resuspended in fresh buffer and incubated again in the microtube shaker under the same conditions. The cumulative release (CR) values were obtained according to eqn (3), with the percentage released DOX (% released(t)) calculated by eqn (4):

$$\%\text{CR} = \%\text{released}(t-1) + \%\text{released}(t) \quad (3)$$

$$\%\text{released} = \frac{[\text{DOX}]_t \cdot (\text{Volume})}{\text{DOX}_{\text{Total}}} \cdot 100 \quad (4)$$

where $[\text{DOX}]_t$ is the concentration of DOX at time t determined by the equation of the calibration curve in Fig. S2 (ESI†) obtained by linear regression (R^2 = 0.987), Volume is 1.5 mL representing the supernatant collected after centrifugation at each time point, and $\text{DOX}_{\text{total}}$ is the amount of DOX in 250 μL of each NC formulation.

Protein corona characterization

First, the amount of adsorbed protein to the NCs was measured by the bicinchoninic acid (BCA) assay. PLGA-DOX, Dex1/PLGA-DOX and Dex5/PLGA-DOX NCs were incubated in medium containing 10% (v/v) FBS and medium without FBS for 2 h at 37 °C. After incubation, the NCs were centrifuged once to remove unbound serum (10 000 g, 20 min, 20 °C) and resuspended in the same volume of ddH_2O. Aliquots of 10 μL were transferred to a 96 well plate with 40 μL of 2% (w/v) sodium dodecyl sulfate and 200 μL of freshly prepared BCA working reagent was added to each well and the plate was incubated at 37 °C for 1 h. Absorbance was measured on a SpectraMax® M3 plate reader (Molecular Devices), controlled by SoftMax Pro software at 562 nm. Bovine serum albumin (BSA) was used as a protein standard to determine the amount of adsorbed protein on the NCs. The protein concentration was calculated by **subtracting** the absorbance of the NCs incubated in medium without FBS, followed also by one centrifugation (10 000 g, 20 min, 20 °C), from the absorbance of each respective formulation incubated in medium containing 10% (v/v) FBS. The assay was repeated three times for the same batches of NCs but exposed separately to FBS for protein adsorption.

For sodium dodecyl sulfate–polyacrylamide gel electrophoresis (SDS-PAGE), the NCs were incubated in media containing 10% (v/v) FBS for 2 h at 37 °C, centrifuged (10 000 g, 20 min, 20 °C) and resuspended in 20 μL of 2× Laemmli buffer (4% (w/v) SDS, 10% (w/v) 2-mercaptoethanol (2-ME), 20% (v/v) glycerol, 0.004% (w/v) bromophenol blue, 0.125 M Tris HCl pH 6.8). The samples were then incubated at 96 °C for 10 min to denature the adsorbed proteins. The NCs were pelleted by centrifugation (10 000 g, 20 min, 20 °C) and 10 μL of the supernatant containing the isolated proteins was loaded to a 10% (v/v) polyacrylamide gel. The gel was resolved at 100 V for 1.5 h and stained with the GelCode™ Blue Stain Reagent following the manufacturer's instructions.

Cell culture

Myocardial cells from the rat heart (H9C2, ATCC) human breast adenocarcinoma cells from the mammary gland (MCF-7, ATCC), and mouse monocyte/macrophage-like cells from ascites (RAW 264.7, ATCC) were cultured in DMEM supplemented with 10% (v/v) FBS in 75 cm^2 flasks at 37 °C in a humidified atmosphere with 5% CO_2. Cells were subcultured at 70–80% confluency. DMEM was originally formulated with gentamicin sulfate (50 mg l^{-1}) and amphotericin B (25 μg mL^{-1}).

Cell viability and cell damage

Cell viability, early apoptotic cell detection and cell membrane damage were assayed by the tetrazolium reduction based colorimetric method, annexin V binding assay using the FITC Annexin V Apoptosis Detection Kit I (#556547) and trypan blue

 This journal is © The Royal Society of Chemistry 2022

Open Access Article. Published on 01 September 2022. Downloaded on 12/29/2025 6:58:32 AM.
This article is licensed under a Creative Commons Attribution 3.0 Unported Licence.

exclusion method, respectively. In tetrazolium reduction based colorimetric assay, (3-(4,5-dimethylthiazol-2-yl)-2,5-diphenyltetrazolium bromide) (MTT, #M2128) is reduced to formazan by the action of NAD(P)H dependent oxidoreductases. The assays were performed in 96 well clear plates with a flat bottom and 5×10^3 cells were seeded per well and grown for 24 h before being exposed to the NCs. PLGA-DOX, Dex1/PLGA-DOX and Dex5/PLGA-DOX NCs were tested with DOX in the concentration range of 1.6–50 μg mL^{-1}. Absorbance was measured on a SpectraMax® M3 plate reader (Molecular Devices), controlled by SoftMax Pro software at 570 and 630 nm.

Annexin V is a Ca^{2+}-dependent phospholipid-binding protein that binds to membrane phosphatidylserine (PS) exposed on early apoptotic cells. The analyses were performed using the FITC Annexin V Apoptosis Detection Kit I. In a 24 well plate, 10^5 cells of each strain were seeded in each well and grown for 24 h. The cells were exposed to the nanocarriers at 1 μg mL^{-1} of DOX for 24 h. The culture medium was removed, the cells were detached from the plate with 0.25% trypsin-EDTA solution, washed by centrifugation (4 °C, 500 g, 10 min) and resuspended in 1× Annexin V Binding Buffer provided with the kit. The cells were stained with 5 μL of Annexin V-FITC conjugate provided with the kit and incubated in the dark for 15 min. The measurements were performed immediately in a BD FACS Callibur™ Flow Cytometer equipped with one laser (488 nm). Emission was measured using FL1 (530/30) and data analysis was performed using FlowJo v10. Trypan blue is a large negatively charged dye that is excluded by viable cells with intact cell membranes while dead cells are stained, due to their damaged membranes. Trypan blue exclusion assays were performed in 48 well clear plates with a flat bottom and 10^5 cells were seeded per well and grown for 24 h before being exposed to the NCs. PLGA-DOX and Dex5/PLGA-DOX NCs were tested with DOX in the concentration range of 0.01–10 μg mL^{-1}. After treatment, the cells were detached from the plate with 0.25% trypsin-EDTA solution and 10 μL aliquots of the sample were mixed with 10 μL of Trypan blue (0.4% (w/v)). The viable cells were counted using a Countess II Automated Cell Counter (Invitrogen).

Internalization assays

Flow cytometry experiments were performed with a BD FACS Callibur™ Flow Cytometer, equipped with an air-cooled argon-ion laser (488 nm). For the experiment, cells were seeded in 24 well plates, at 10^5 cells per well and grown for 24 h. Cells were exposed to DOX loaded NCs for 2 or 4 h at 37 °C, 5% CO_2. Following incubation, the medium containing the NCs was removed, cells were washed with 1× PBS (pH 7.4) and detached from the plate with 0.25% trypsin-EDTA solution. The samples were centrifuged (4 °C, 500 g, 10 min) and washed with Sheath Fluid (BD Bioscience) supplemented with 0.5% (w/v) bovine serum albumin. Emission was measured using FL2 (585/42) and data analysis was performed using FlowJo v10. For the inhibition studies, cells were incubated for 30 min with amiloride (100 μg mL^{-1}), nystatin (40 μg mL^{-1}), nocodazole (10 μg mL^{-1}), hydroxy-dynasore (100 μmol l^{-1}), dansyl-cadaverine (100 μmol l^{-1}), heparin (10 units mL^{-1}), dextran (2 mg mL^{-1}) and dextran sulfate (5 μg mL^{-1}) prior to incubation with the NCs for 2 h.

Reactive oxygen species (ROS)

ROS detection was performed based on oxidation of 2′-7′-dichlorodihydrofluorescein diacetate (CM-H_2DCFDA). Cells were seeded in a 24 well plate at 10^5 cells of each strain per well, and grown for 24 h. The cells were exposed to nanocarriers at 12.5 μg mL^{-1} of DOX for 2 h, washed with PBS (pH 7.4) and incubated with 10 μmol L^{-1} CM-H_2DCFDA in DMEM culture medium without phenol for 30 minutes. The culture medium was removed, the cells were detached from the plate with 0.25% trypsin-EDTA solution or cell scraper, washed by centrifugation (4 °C, 500 g, 10 min) and resuspended in Sheath Fluid (BD Bioscience) supplemented with 0.5% (w/v) bovine serum albumin. All measurements were performed in a BD FACS Callibur™ Flow Cytometer equipped with one laser (488 nm). Excitation was measured using FL1 (530/30) and data analysis was performed using FlowJo v10.

Statistics

Statistical analyses were performed using ANOVA with Tukey's *post hoc* test using the software Origin Pro 8. The significance level was 0.05. **p*-value < 0.05, ***p*-value < 0.01 and ****p*-value < 0.001.

Results and discussion

Effect of dextran on the properties of DOX loaded PLGA NCs

The size distributions of DOX-loaded PLGA nanocarriers prepared in the absence or presence of dextran were measured by dynamic light scattering (DLS), nanotracking analysis (NTA) and transmission electron microscopy (TEM) (Fig. 1a–f). The NC sizes are homogeneously distributed (PdI < 0.2, Table 1) and size populations are represented in Fig. 1a (PLGA-DOX NCs), Fig. 1b (Dex1/PLGA-DOX NCs) and Fig. 1c (Dex5/PLGA-DOX NCs), and corroborated by TEM images (Fig. 1d–f). Zeta potential (ζ-potential) was also determined for all formulations and confirmed the negative surface charge (Table 1) due to carboxyl end groups in PLGA. Analysis of the dextran content in the NCs was performed by NMR spectroscopy and showed that the mole fraction of (1 → 6)-α-D-glucose monomers from dextran and PLA monomers was 8.2 and 1.7 mol% for Dex5/PLGA-DOX and Dex1/PLGA-DOX NCs, respectively (Fig. S8, ESI†).

The NC concentration –number of particles per ml – was estimated using NTA and Dex1/PLGA-DOX NCs exhibited a higher particle yield (Table 1 and Fig. 1g) which may be explained by dextran-Pluronic®-F127 distribution between solvents during emulsion. Above a certain concentration, dextran/Pluronic®-F127 solution separates into two phases, with Pluronic®-F127 partitioning into a dextran continuous phase.[29] PLGA preferably partitions into the Pluronic®-F127 phase due to the amphiphilic properties of Pluronic®-F127 and the partial solubility of ethyl acetate in water, but it can also form multiple emulsions.[29] The ratio of the Pluronic®-F127/dextran aqueous

Open Access Article. Published on 01 September 2022. Downloaded on 12/29/2025 6:58:32 AM.
This article is licensed under a Creative Commons Attribution 3.0 Unported Licence.

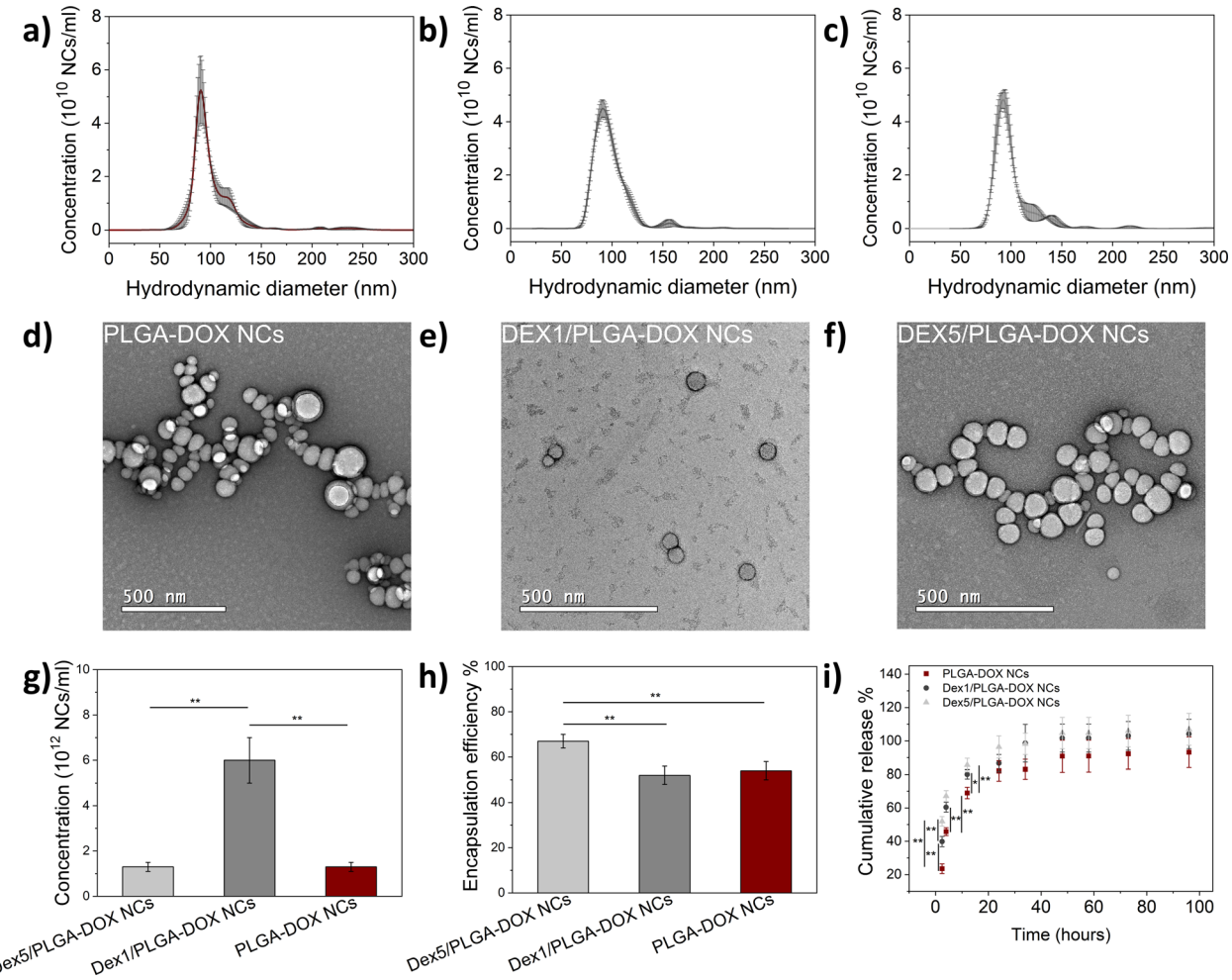

Fig. 1 Characterization of the PLGA-DOX, Dex1/PLGA-DOX and Dex5/PLGA NCs. NTA size distribution of (a) PLGA-DOX NCs, (b) Dex1/PLGA-DOX NCs and (c) Dex5/PLGA-DOX NCs with respective representative TEM images in (d), (e) and (f). (g) Particle yield (number of NCs per ml), (h) encapsulation efficiency and (i) cumulative release profile in 1× PBS at pH 7.4 and 37 °C of PLGA-DOX, Dex1/PLGA-DOX and Dex5/PLGA NCs. Statistical analysis was performed using ANOVA with Tukey's *post hoc* test. The values represent mean ± S.D. (n = 4). *p-value < 0.05 and **p-value < 0.01.

Table 1 Characterization of DOX-loaded PLGA nanocarriers with and without dextran. NTA size (diameter), Z-average (PdI), TEM size (diameter), ζ potential, particle concentration and encapsulation efficiency of the NCs synthesized with and without dextran. Statistical analysis was performed using ANOVA with Tukey's *post hoc* test. The values represent mean ± S.D. of independent syntheses (n = 4)

Nanocarrier	NTA size (nm) (D90)	Z-Average (nm) (PdI)	TEM size (nm)	Zeta potential (mV)	Concentration (10^{12} NCs mL^{-1})	Encapsulation efficiency (EE) (%)
Dex5/PLGA-DOX NCs	101 ± 30 (129 ± 6)	127 ± 26 (0.19)	115 ± 29	−38 ± 4	1.3 ± 0.2^{b}	67 ± 3^{ab}
Dex1/PLGA-DOX NCs	102 ± 28 (129 ± 3)	111 ± 13 (0.11)	66 ± 17	−35 ± 3	6 ± 1^{a}	52 ± 4
PLGA-DOX NCs	107 ± 28 (132 ± 11)	114 ± 10 (0.07)	83 ± 27	−36 ± 7	1.3 ± 0.2^{b}	54 ± 4

^{a} Significantly different from PLGA-DOX NCs with p-value < 0.05. ^{b} Significantly different from Dex1/PLGA-DOX NCs with p-value < 0.05.

two-phase system affects PLGA emulsion and particle structure which may form core–shell or composite particles.[29]

Loading and release of DOX were evaluated with UV-visible and fluorescence spectroscopy. For Dex5/PLGA-DOX NCs, a significant increase in the encapsulation efficiency (EE) was observed when compared to Dex1/PLGA-DOX and PLGA-DOX NCs (Table 1 and Fig. 1h). Encapsulation efficiency (EE) is affected by the type and concentration of the stabilizing agent in emulsions.[30] The use of surfactants in drug encapsulation by double emulsion is critical as a barrier to drug release at the internal interface, and, at the external interface, as a steric stabilizer.[31] By adding Tween 20 or Tween 60 to the external

 This journal is © The Royal Society of Chemistry 2022

Open Access Article. Published on 01 September 2022. Downloaded on 12/29/2025 6:58:32 AM.
This article is licensed under a Creative Commons Attribution 3.0 Unported Licence.

aqueous phase of polybutyl adipate (PBA) nanocapsules prepared by double emulsion, Khoee and Yaghoobian reported that the higher viscosity of the external aqueous phase and the reduced diffusion of the hydrophilic cargo increased the encapsulation efficiency of penicillin-G.[31] PLGA MPs formed by the emulsion of 0.0625% PLGA in the 2% Pluronic®-F127/10% dextran aqueous two-phase system have a core–shell morphology with Pluronic®-F127 concentrated in the core and dextran concentrated in the shell, as reported by Yeredla *et al.*[29] Thus, the increase of EE for Dex5/PLGA-DOX NCs may be a consequence of the dextran arrangement at the NC shell preventing DOX diffusion to the external aqueous phase during emulsion preparation.

Cumulative release (Fig. 1i) revealed higher release rates for Dex1/PLGA-DOX and Dex5/PLGA-DOX NCs compared to PLGA-DOX NCs at 2.5, 4 and 12 h, indicating an increase in the burst release for the dextran-containing formulations. Dextran solubility in water may maximize the interactions of NCs with water molecules, favoring the penetration of the solvent in the nanocarrier hydrophobic core, intensifying the release.[32–34]

Dextran modulates protein corona formation and hinders uptake by non-phagocytic cells

In vitro cellular uptake studies were performed with H9C2, MCF-7 and RAW 264.7 by flow cytometry. H9C2 and MCF-7 were incubated for 4 h at 37 °C with free DOX, PLGA-DOX, Dex1/PLGA-DOX and Dex5/PLGA NCs. RAW 264.7 cells were exposed to the same samples for 2 and 4 h at 37 °C. The initial DOX dosage was equivalent for all groups (12.5 μg mL^{-1}).

A comparison of the fluorescence intensities in Fig. 2 indicated a significant reduction in Dex5/PLGA-DOX NC uptake by MCF-7 (Fig. 2a) and H9C2 (Fig. 2b), non-phagocytic cells, when compared to PLGA-DOX NCs and Dex1/PLGA-DOX NCs. In contrast, RAW 264.7, a phagocytic cell, showed higher uptake of Dex5/PLGA-DOX NCs in 2 h (Fig. 2c). It has been shown that dextran-coated NCs efficiently target macrophages[35,36] and recently, Q. Chen *et al.* demonstrated that dextran-coated PLGA NCs have increased uptake in macrophages due to receptor mediated endocytosis.[37] C-type lectins like SIGN-R1 and mannose receptors (CD206) are expressed in macrophages and mediate Dex uptake, as well as scavenger receptor type 1 (SR-A1), highly expressed in RAW 264.7. These biomolecules may be responsible for triggering Dex5/PLGA-DOX NC internalization in RAW 264.7 cells.[38–43] Competition with free Dex (20 μg mL^{-1}) reduced the uptake of Dex5/PLGA-DOX NCs (Fig. 2g), supporting the hypothesis of receptor mediated endocytosis. However, Dex1/PLGA-DOX NC uptake was not significantly different from that of PLGA-DOX NCs in 2 h and also no significant difference was observed in the uptake of Dex1/PLGA-DOX NCs in the presence and absence of free Dex (Fig. 2g). In addition, no significant difference was observed between any of the tested formulations after 4 h of incubation with the NCs (Fig. S5a, ESI†).

In biological environments (mimicked *in vitro* by FBS rich medium), proteins bind to the NCs forming protein corona (PC) affecting cell uptake.[10,12,44–46] To study the influence of PC on NC uptake, MCF-7, H9C2 and RAW 264.7 cells were incubated for 2 h at 37 °C with PLGA-DOX, Dex1/PLGA-DOX and Dex5/PLGA-DOX NCs in medium without FBS. Dex1/PLGA-DOX NC uptake by MCF-7 and H9C2 was reduced in the absence of FBS compared to PLGA-DOX NC uptake (Fig. 2d and e), which is not observed in the presence of serum. However, RAW 264.7 showed higher uptake of Dex5/PLGA-DOX NCs in medium without FBS (Fig. 2f), similar to the uptake in the presence of serum (Fig. 2c). To characterize the protein corona (PC) formed on PLGA-DOX, Dex1/PLGA-DOX and Dex5/PLGA-DOX NCs, we incubated the NCs in media containing 10% FBS for 2 h at 37 °C. The absorbed protein amount was measured by BCA assay (Fig. 2i) and the PC molecular composition was studied by SDS-PAGE (Fig. 2f). The SDS-PAGE gel image (Fig. 2h) showed that the NCs' PC is formed by proteins with a range of densities. An increase in the Dex amount led to a decrease in the lane intensity, corroborating the results from the BCA assay. Two band sizes are very distinct for the protein corona, one relative to serum albumin and globulins, the major components of FBS, with sizes around 55–70 kDa, and the other, most likely relative to apolipoprotein C (~10 kDa).[47]

Surface modifications influence the composition and thickness of protein corona, affecting the uptake of NCs.[11,46] Dextran can reduce the interaction of NPs with serum proteins and higher amounts of dextran on chitosan-based NPs diminished the hard corona around them.[12] In addition, the Dex ability of preventing protein adsorption is well known in the scientific community.[48–51] Sakulkhu *et al.* reported that the serum proteins adsorb to a greater extent onto PVA-coated superparamagnetic iron oxide nanoparticles (SPIONs) than onto dextran-coated SPIONs, and that negatively charged dextran-coated SPIONs' protein corona was formed specifically by alpha-1-antiproteinase, thyroxine-binding globulin, endopin-1, fetuin-B, transthyretin, hemoglobin subunit alpha, and apolipoprotein A-II.[52] Thus, the protein adsorption onto NCs prepared with 5% (w/v) Dex is reduced compared to the Dex1/PLGA-DOX NCs, which exhibit higher intracellular accumulation attributed to PC formation, suggesting that protein adsorption is dependent on the dextran amount. Such dependence has already been reported by Tekie *et al.*, who showed that higher amounts of dextran diminished hard corona formation in chitosan-based nanoparticles.[12] Corona formation may also mask ligands. Corona formation may also mask ligand-functionalization on the particle surface, limiting its targeting abilities.[8,9,53,54] The surface functionalization masking effect may be observed for the Dex1/PLGA-DOX NCs when uptake studies are performed in the presence of FBS (Fig. 2a).

To elucidate the differences in NC uptake, the main endocytic pathways were assessed using pharmacological inhibitors for PLGA-DOX NCs (Fig. S5b, ESI†) and Dex5/PLGA-DOX NCs (Fig. S5c, ESI†) in MCF-7 cells. Uptake was decreased by amiloride, hydroxy-dynasore and dansyl-cadaverine inhibition of macropinocytosis and clathrin-mediated endocytosis, respectively, for both NCs with and without Dex. Non-targeted spherical nanoparticles with ~100 nm are mainly internalized by clathrin-dependent endocytosis[55] while dextran is used as a macropinocytosis marker.[56] However, the dextran endocytic pathway may vary with molecular weight.[57] In HeLa cells,

Open Access Article. Published on 01 September 2022. Downloaded on 12/29/2025 6:58:32 AM.
This article is licensed under a Creative Commons Attribution 3.0 Unported Licence.

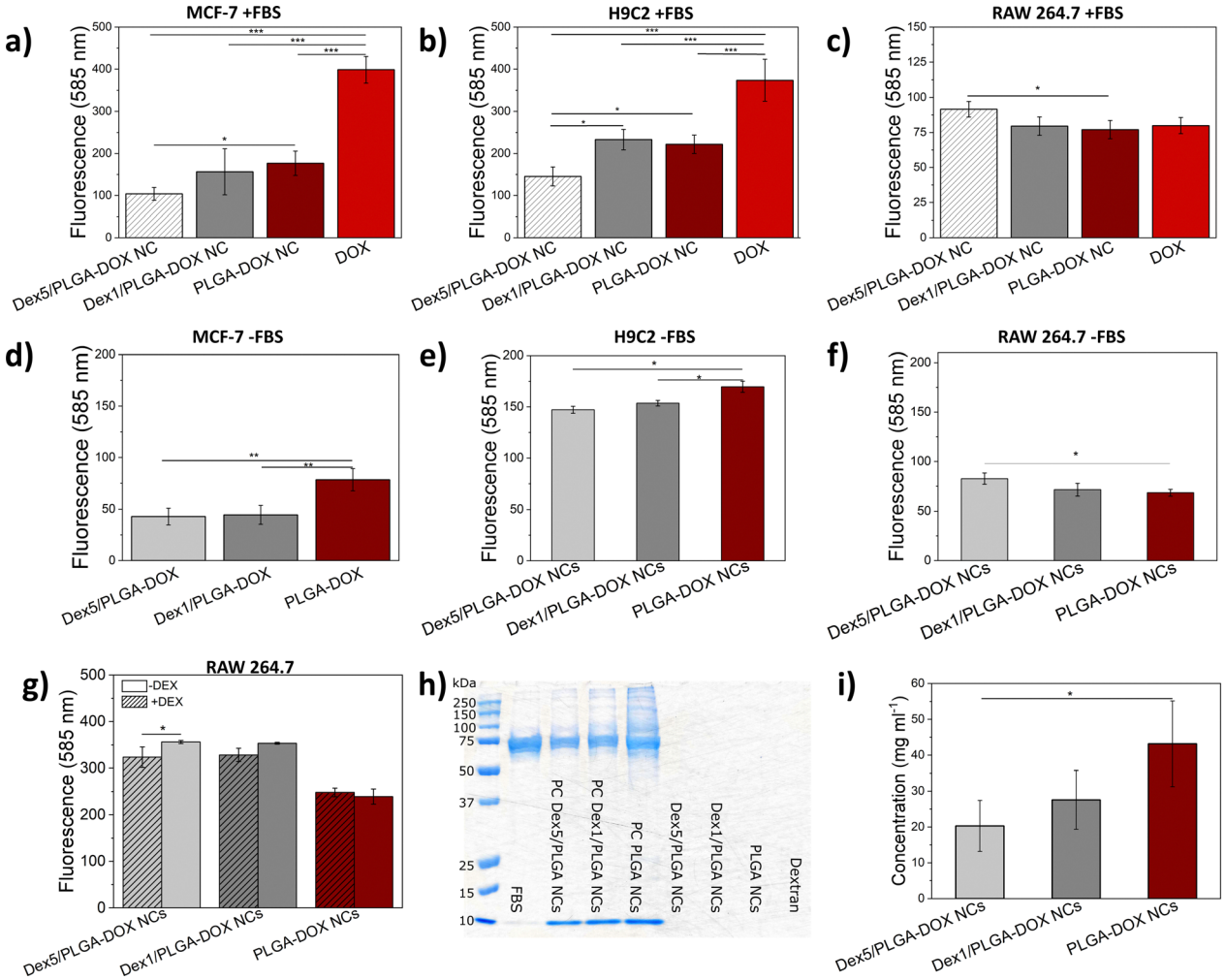

Fig. 2 *In vitro* cellular uptake of PLGA-DOX, Dex1/PLGA-DOX and Dex5/PLGA NCs by flow cytometry analysis. Comparison of cell fluorescence of (a) MCF-7 and (b) H9C2 incubated for 4 h and (c) RAW 264.7 incubated for 2 h at 37 °C with DOX, PLGA-DOX, Dex1/PLGA-DOX and Dex5/PLGA-DOX NCs. Uptake by (d) MCF-7, (e) H9C2 and (f) RAW 264.7 in the absence of FBS. MCF-7, H9C2 and RAW 264.7 were incubated for 2 h at 37 °C with PLGA-DOX, Dex1/PLGA-DOX and Dex5/PLGA-DOX NCs in medium without FBS. DOX dosage was 12.5 μg mL^{-1} for all analyses. (g) Uptake of Dex5/PLGA-DOX, Dex1/PLGA-DOX and PLGA-DOX NCs by RAW 264.7 in the presence of an excess of Dex (20 μg mL^{-1}). Characterization of protein corona formed on PLGA-DOX, Dex1/PLGA-DOX and Dex5/PLGA-DOX NCs incubated for 2 h in media containing 10% (v/v) FBS at 37 °C. (h) Adsorbed protein amount measured by the bicinchoninic acid (BCA) assay. (i) SDS-PAGE gel image of the proteins recovered from protein corona formed on PLGA-DOX, Dex1/PLGA-DOX and Dex5/PLGA-DOX NCs (FBS concentration was 1% (v/v)). Statistical analysis was performed using ANOVA with Tukey's *post hoc* test. The values represent mean ± S.D. (n = 3, n = 4). *p-value < 0.05, **p-value < 0.01, and ***p-value < 0.001.

dextran 70 kDa enters the cells by clathrin- and dynamin-independent micropinocytosis while dextran 10 kDa is internalized by clathrin- and dynamin-dependent endocytosis in addition to macropinocytosis.[57] Nevertheless, inhibition of clathrin-dependent and -independent endocytosis and macropinocytosis had no effect on dextran-based doxorubicin nanocarrier uptake.[18] Some authors suggested that dextran-coated NCs are mainly internalized by fluid phase endocytosis pathways, without the mediation of a receptor.[58,59] Noteworthily, aldehyde-functionalized dextran-based nanocarrier systems are not affected by inhibition of clathrin-dependent and -independent endocytosis, micropinocytosis and membrane cholesterol depletion in SK-N-BE cells, a human neuroblastoma cell line, but they are affected by glucose content in the medium, as well as concanavalin A, while MRC-5 cells seem to be indifferent to both treatments.[18] The latter highlights the fact that nanoparticle internalization depends not only on the particle properties, *e.g.*, size and surface, but also on the cell type.[49,50]

We investigated whether heparan sulfate proteoglycan (HSPG) acts as a receptor for the NCs, by competitive inhibition with free heparin. HSPG is a cell-surface receptor that is involved in the uptake of diverse macromolecular cargoes and plays a role in various diseases such as cancer.[60,61] Incubation of MCF-7 with the NCs in the presence of heparin did not diminish NC uptake compared to incubation in the absence of heparin, indicating that HSPG does not participate in NC uptake. Also, competitive inhibition with free Dex did not affect the uptake of NCs capped with the polysaccharide, which indicates that the uptake is not receptor-mediated in MCF-7. Dextran interaction with the cell membrane of non-phagocytic

 This journal is © The Royal Society of Chemistry 2022

Open Access Article. Published on 01 September 2022. Downloaded on 12/29/2025 6:58:32 AM. This article is licensed under a Creative Commons Attribution 3.0 Unported Licence.

cells may limit NC–cell adhesion and affect non-receptor mediated endocytosis, which is supported by competitive assay in the presence of free Dex.[40,58,59,62] In addition, dextran coatings are shown to avoid non-specific hydrophobic interactions and reduce cell adhesion between dextran coating and cell membrane,[48,63] which supports the hypothesis that the uptake is not receptor-mediated in MCF-7. Similar results were reported for the uptake of superparamagnetic NPs coated with dextran by HeLa cells.[59]

Dextran-containing formulations induce cell membrane damage

All NC formulations presented a sustained-release profile with most of the DOX being released during the first 30 h. This correlates with the cell viability of MCF-7 (Fig. 3a, c and Fig. S3a, ESI†), H9C2 (Fig. 3b, d and Fig. S3b, ESI†) and RAW 264.7 (Fig. S3c, ESI†) assessed by MTT and Trypan Blue exclusion assays. The cells were incubated with PLGA-DOX, Dex1/PLGA-DOX and Dex5/PLGA-DOX NCs at 37 °C for 24 and 48 h. Viability was clearly lower after 48 h incubation, when compared to 24 h (Fig. S3, ESI†), which agrees with the release of DOX showed in the release profile (Fig. 1i) and the half-life of DOX-DNA covalent lesions, known to be 5–40 h.[64,65] Also, all formulations were shown to be more effective against breast cancer cells, MCF-7, when compared to their effect on myoblasts from heart tissue, H9C2, and macrophages, RAW 264.7.

Non-significant difference in cell viability was observed between NC formulations as assessed by MTT (Fig. 3a and b). However, by trypan blue exclusion assay (Fig. 3c and d) and annexin V binding assay (Fig. 3e and f) it was possible to observe a reduced viability of MCF-7 and H9C2 treated with Dex5/PLGA-DOX NCs in comparison to treatment with PLGA-DOX NCs. The choice of the best method to assess cell damage caused by drug carrier formulations depends on the mechanism of damage and location of its direct target.[66,67] MTT assay assesses the mitochondrial function by measuring the activity of mitochondrial dehydrogenase enzymes while annexin V specifically binds to exposed phosphatidylserine (PS) in early apoptotic cells.[68,69] Trypan blue exclusion assay evaluates cell membrane integrity by accounting for dead cells that took up trypan blue, a negatively charged dye excluded by live cells.[69] Apoptosis is a normal genetically programmed process for removal of unwanted cells.[68,70] However, cancer cells express anti-apoptotic genes that allow them to survive longer, favoring tumor growth and drug resistance.[70,71] One of the earliest features of apoptosis is the loss of membrane asymmetry and translocation of phosphatidylserine (PS) from the inner side of the plasma membrane to the surface. Annexin V specifically binds to exposed PS in early apoptotic cells.[68] Annexin V binding assay showed that Dex5/PLGA-DOX NC treatment leads to higher amounts of early apoptotic cells than PLGA-DOX and Dex1/PLGA-DOX NC treatment.

PS translocation precedes the loss of membrane integrity, which occurs in later stages of cell death in both apoptotic and necrotic processes.[61] Thus, it is common to stain the cells with annexin V together with 7-aminoactinomycin D (7-AAD) or propidium iodide (PI), which are fluorescent compounds that intercalate in DNA and can only pass through damaged cell membranes.[68,72] However, the fluorescence spectrum of DOX overlaps with the spectra of both dyes, and only staining with annexin V was evaluated.[73] Therefore, we assessed the membrane integrity by the trypan blue exclusion assay. Despite both Dex5/PLGA-DOX and PLGA-DOX NCs have decreased cell viability after 48 h exposure, the NCs prepared with 5% (w/v) Dex may have induced greater membrane damage levels, corroborating the results of annexin V apoptosis detection. Although MTT assay is commonly used to verify cytotoxicity *in vitro*, this test has known limitations for assessing nanomaterial toxicity.[74–80] MTT assay can mislead cell viability results due to optical interference.[81–83] For example, MTT assay is reported to overestimate the viability of CHO-K1 cells treated with nanoscale TiO_2 when compared to trypan blue exclusion assay because nanoscale TiO_2 induces O_2^{2-} formation and reduces MTT.[77] The viability of bovine peripheral blood mononuclear cells exposed to $K_2Cr_2O_7$ evaluated by MTT did not match trypan blue exclusion assay due to ROS interference in the MTT results.[84] Superoxide ions can reduce tetrazolium salts and produce the absorbent formazan; therefore MTT assay may not be representative of toxicity of nanomaterials for which induction of oxidative stress is a key toxicity mechanism.[77,84,85]

Dex5/PLGA-DOX NCs induce oxidative stress in MCF-7 and H9C2

To evaluate ROS production, free DOX, Dex5/PLGA-DOX, Dex1/PLGA-DOX and PLGA-DOX NCs were incubated for 2 h at 37 °C with MCF-7, H9C2 and RAW 264.7 cells, and ROS generation was detected by oxidation of 2′-7′-dichlorohydrofluorescein diacetate (CM-H_2DCFDA) using flow cytometry. DOX dosage was the same for all experimental groups (12.5 μg mL^{-1}). Although free dextran 40 exhibits hydrogen peroxide scavenging activity,[86] Dex5/PLGA-DOX NCs induced higher generation of reactive oxygen species (ROS) in MCF-7 (Fig. 4a) and H9C2 (Fig. 4b) compared with Dex1/PLGA-DOX, PLGA-DOX NCs and free DOX. Oxidative stress is one of the main DOX toxicity mechanisms,[1] which might explain the increased generation of ROS associated with the larger amount of DOX per particle. It has been reported that faster iron ion release by dextran-coated iron oxide nanoparticles (IONs) may contribute to the generation of ROS compared to PEG-coated IONs, as observed for Dex5/PLGA-DOX NCs (Fig. 1i) where dextran favors water infiltration accelerating NC degradation.[87,88]

RAW 264.7 presented similar ROS generation for the NCs with and without dextran (Fig. 4c). It was also observed that higher ROS levels were induced by the NCs than by free DOX, which may be due to inflammation-induced oxidative stress.[26] Macrophages, as professional phagocytic cells, can induce ROS upon NP uptake *via* the NADPH oxidase enzyme system.[89]

Despite the reduced uptake, Dex5/PLGA-DOX NCs showed higher ROS levels in heart cells indicating that NCs prepared with 5% (w/v) of dextran may cause long-term adverse effects such as irreversible cardiomyopathy and heart failure, induced by oxidative stress.[1,2,87] Dextran-coated IONs formerly reported to be safe for stem and other non-neuronal cell types were

Open Access Article. Published on 01 September 2022. Downloaded on 12/29/2025 6:58:32 AM.
This article is licensed under a Creative Commons Attribution 3.0 Unported Licence.

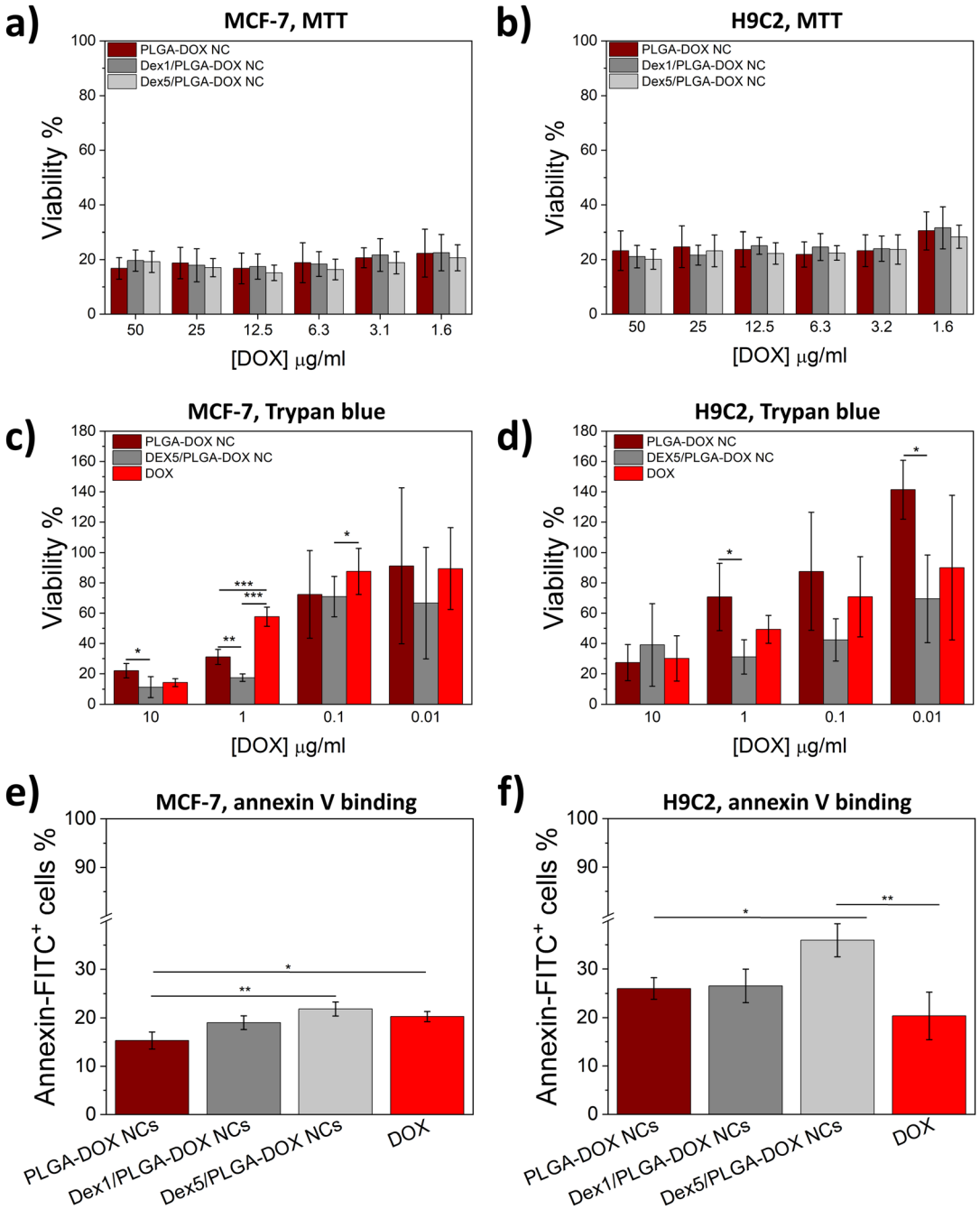

Fig. 3 Evaluation of cell viability by MTT, Trypan Blue and annexin V binding assay for NCs prepared in the presence and absence of dextran 40. Viability of (a) MCF-7 and (b) H9C2 incubated for 48 h at 37 °C with PLGA-DOX, Dex1/PLGA-DOX and Dex5/PLGA NCs by MTT assay. Viability of (c) MCF-7 and (d) H9C2 incubated for 48 h at 37 °C with PLGA-DOX, Dex1/PLGA-DOX and DOX by trypan blue assay. Viability of (e) MCF-7 and (f) H9C2 incubated for 24 h at 37 °C with PLGA-DOX, Dex1/PLGA-DOX and DOX by annexin V binding assay. Statistical analysis was performed using ANOVA with Tukey's *post hoc* test. The values represent mean ± SD (n = 4). *p-value < 0.05, **p-value < 0.01, and ***p-value < 0.001.

found to be toxic to neurons, mainly due to oxidative stress.[22] In addition, dextran-coated SPIONs showed genotoxicity caused by oxidative stress at non-cytotoxic concentrations in HepG2 cells.[23]

The effects of oxidative stress include DNA damage, mitochondrial dysfunction and membrane damage due to lipid peroxidation.[24] Lipid peroxidation inhibits membrane functions by modifying the dielectric constant and contributing to the depolarization of the membrane potential, which lead to loss of membrane barrier properties and cell death. Also, lipid peroxidation products are highly reactive and can change the structure and function of membrane proteins, cytoplasmic enzymes and nucleic acids.[25]

Our results suggest that higher concentrations of dextran, 5% (w/v), added to DOX-loaded PLGA NC emulsion formulations as a stabilizing and capping agent may induce higher

 This journal is © The Royal Society of Chemistry 2022

Open Access Article. Published on 01 September 2022. Downloaded on 12/29/2025 6:58:32 AM.
This article is licensed under a Creative Commons Attribution 3.0 Unported Licence.

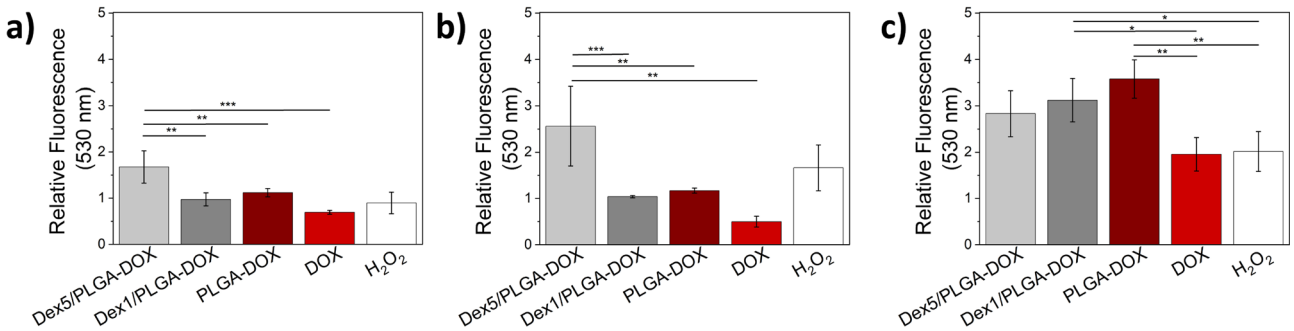

Fig. 4 ROS studies to evaluate oxidative stress induced by free DOX, Dex5/PLGA-DOX, Dex1/PLGA-DOX, and PLGA-DOX NCs. Flow cytometry detection of ROS by oxidation of 2′-7′-dichlorodihydrofluorescein diacetate (CM-H_2DCFDA) in (a) MCF-7, (b) H9C2 and (c) RAW 264.7 cell lines after incubation for 2 h at 37 °C with the NCs. Statistical analysis was performed using ANOVA with Tukey's *post hoc* test. The values represent mean ± SD (n = 4). *p-value < 0.05, **p-value < 0.01, and ***p-value < 0.001.

degree of toxicity than formulations with lower concentrations, 1% (w/v) or without dextran, in breast cancer and myocardial cells. The results are evidenced by ROS imbalance and oxidative membrane damage assessed by trypan blue exclusion and annexin V binding assays, but do not correlate with higher uptake. DOX-induced toxicity is largely associated to mitochondrial dysfunction; however, MTT assay did not indicate difference in mitochondrial activity between the NCs. Altogether, the results indicate that toxicity of Dex5/PLGA-DOX NCs is associated with oxidative membrane damage. Accumulative ROS production from mitochondrial and non-mitochondrial sources may facilitate disruption of homeostasis and improve cancer treatment where Dex5/PLGA-DOX NCs would benefit cancer treatment. However, it may also aggravate adverse effects such as irreversible cardiomyopathy and heart failure caused by oxidative stress.[1,2,87] For future direction, tumor accumulation and reparative action of cardiac tissue treated with Dex-containing formulations need to be addressed; nonetheless it is clear that dextran modulation may benefit cancer therapy.

These results highlight the importance of an in-depth investigation of the NC–cell interaction considering the mechanisms of damage. The specificity of the toxicity tests must also be considered, since effects including DNA and membrane damage, oxidative stress, and mitochondrial dysfunction can be posed without detectable changes in cytotoxicity assessed by MTT assays.[23,26]

Conclusions

The DOX loaded PLGA NCs were prepared by the emulsion diffusion method using Pluronic®-F127 and 0, 1 and 5% (w/v) dextran (Dex) as stabilizing agents. The Dex5/PLGA-DOX NCS showed an increased encapsulation efficiency when compared with Dex1/PLGA-DOX and PLGA-DOX NCs attributed to the Dex arrangement at the NC shell preventing DOX diffusion to the external aqueous phase during emulsion preparation. Dex5/PLGA-NCs revealed a reduced uptake by myocardial and breast adenocarcinoma cells, as also observed for Dex1/PLGA-DOX NCs in the absence of serum, suggesting that protein corona formation is modulated by the amount of dextran in the formulation which was supported by BCA assay and SDS-PAGE of the NCs in the presence of serum. Competitive inhibition with free dextran did not affect the uptake of NCs capped with the polysaccharide in breast adenocarcinoma cells, supporting the hypothesis that the uptake is not receptor-mediated in non-phagocytic cells. RAW 264.7 expresses C-type lectins and scavenger receptors that can mediate Dex uptake, justifying the enhanced uptake of Dex5/PLGA-DOX NCs by this cell line.

All the NCs affect cell viability to the same extent when assessed by MTT; however, Dex5/PLGA-DOX NCs induced greater membrane damage in MCF-7 and H9C2. Nanoparticle-induced damage is not limited to mitochondrial dysfunction, but other mechanisms, *e.g.*, membrane and DNA damage, also correlate with cell death. The higher percentage of early apoptotic cells and membrane-damaged cells triggered by Dex5/PLGA-DOX NCs is correlated with their greater induction of ROS, revealing that membrane damage may be posed by oxidative stress. Since irreversible cardiomyopathy and heart failure are mainly induced by oxidative stress, Dex5/PLGA-DOX may contribute more to the long-term adverse effects than formulations with lower Dex concentrations or without Dex.

Author contributions

LCA: conceptualization, investigation, data curation, formal analysis, methodology, project administration, validation, visualization, writing –original draft, writing – review & editing. LR: conceptualization, investigation, data curation, formal analysis, supervision, methodology, project administration, validation, visualization, writing – original draft, writing – review & editing. PMPL: investigation, methodology, writing – review & editing. VZ: funding acquisition, supervision, writing – original draft, writing – review & editing. All authors have given approval to the final version of the manuscript.

Conflicts of interest

There are no conflicts to declare.

Open Access Article. Published on 01 September 2022. Downloaded on 12/29/2025 6:58:32 AM.
This article is licensed under a Creative Commons Attribution 3.0 Unported Licence.

Acknowledgements

LCA was supported by the São Paulo Research Foundation (FAPESP) (Grant numbers 2020/02386-7) and by the Brazilian National Council for Scientific and Technological Development (CNPq) (project number 12085712017-0). LR was supported by the Coordenação de Aperfeiçoamento de Pessoal de Nível Superior – Brasil (CAPES) – Finance Code 001. PMPL was supported by the São Paulo Research Foundation (FAPESP) (Grant numbers 2017/21869-6 and 2020/00124-5) and by the Brazilian National Council for Scientific and Technological Development (CNPq) (project number 309943/2020-5 and 442690/2020-7). We acknowledge the facilities of the Central de Análises Químicas Instrumentais (CAQI) of the São Carlos Institute of Chemistry (IQSC) for the support and assistance in the use of the transmission electron microscope (FAPESP Grant number 2009/54216-9) and 400 MHz NMR.

References

1 C. F. Thorn, C. Oshiro, S. Marsh, T. Hernandez-Boussard, H. McLeod, T. E. Klein and R. B. Altman, *Pharmacogenet. Genomics*, 2011, **21**, 440–446.
2 N. Zhao, M. C. Woodle, A. J. Mixson, U. States and B. Corp, *J. Nanomed. Nanotechnol.*, 2018, **9**(5), 519.
3 F. Danhier, E. Ansorena, J. M. Silva, R. Coco, A. Le Breton and V. Préat, *J. Controlled Release*, 2012, **161**, 505–522.
4 A. Kumari, S. K. Yadav and S. C. Yadav, *Colloids Surf., B*, 2010, **75**, 1–18.
5 S. Tenzer, D. Docter, J. Kuharev, A. Musyanovych, V. Fetz, R. Hecht, F. Schlenk, D. Fischer, K. Kiouptsi, C. Reinhardt, K. Landfester, H. Schild, M. Maskos, S. K. Knauer and R. H. Stauber, *Nat. Nanotechnol.*, 2013, **8**, 772–781.
6 E. Cendrowicz, Z. Sas, E. Bremer and T. P. Rygiel, *Cancers*, 2021, **13**(8), 1946.
7 H. Zhang, A. Xu, X. Sun, Y. Yang, L. Zhang, H. Bai, J. Ben, X. Zhu, X. Li, Q. Yang, Z. Wang, W. Wu, D. Yang, Y. Zhang, Y. Xu and Q. Chen, *Circ. Res.*, 2020, **127**, 610–627.
8 W. Xiao, Y. Wang, H. Zhang, Y. Liu, R. Xie, X. He, Y. Zhou, L. Liang and H. Gao, *Biomaterials*, 2021, **274**, 120888.
9 A. Salvati, A. S. Pitek, M. P. Monopoli, K. Prapainop, F. B. Bombelli, D. R. Hristov, P. M. Kelly, C. Åberg, E. Mahon and K. A. Dawson, *Nat. Nanotechnol.*, 2013, **8**, 137–143.
10 S. Ritz, S. Schöttler, N. Kotman, G. Baier, A. Musyanovych, J. Kuharev, K. Landfester, H. Schild, O. Jahn, S. Tenzer and V. Mailänder, *Biomacromolecules*, 2015, **16**, 1311–1321.
11 V. Francia, K. Yang, S. Deville, C. Reker-Smit, I. Nelissen and A. Salvati, *ACS Nano*, 2019, **13**, 11107–11121.
12 F. S. M. Tekie, M. Hajiramezanali, P. Geramifar, M. Raoufi, R. Dinarvand, M. Soleimani and F. Atyabi, *Sci. Rep.*, 2020, **10**, 9664.
13 L. Shi, J. Zhang, M. Zhao, S. Tang, X. Cheng, W. Zhang, W. Li, X. Liu, H. Peng and Q. Wang, *Nanoscale*, 2021, **13**, 10748–10764.
14 B. Pelaz, P. Del Pino, P. Maffre, R. Hartmann, M. Gallego, S. Rivera-Fernández, J. M. De La Fuente, G. U. Nienhaus and W. J. Parak, *ACS Nano*, 2015, **9**, 6996–7008.
15 C. Qian, Y. Wang, Y. Chen, L. Zeng, Q. Zhang, X. Shuai and K. Huang, *Biomaterials*, 2013, **34**, 6175–6184.
16 K. Alhareth, C. Vauthier, F. Bourasset, C. Gueutin, G. Ponchel and F. Moussa, *Eur. J. Pharm. Biopharm.*, 2012, **81**, 453–457.
17 W. Jie Ma, X. Bo Yuan, C. Sheng Kang, T. Su, X. Yan Yuan, P. Yu Pu and J. Sheng, *Carbohydr. Polym.*, 2008, **72**, 75–81.
18 S. M. Sagnella, H. Duong, A. MacMillan, C. Boyer, R. Whan, J. A. McCarroll, T. P. Davis and M. Kavallaris, *Biomacromolecules*, 2014, **15**, 262–275.
19 N. C. Reichardt, M. Martín-Lomas and S. Penadés, *Chem. Commun.*, 2016, **52**, 13430–13439.
20 J. Hardwicke, E. L. Ferguson, R. Moseley, P. Stephens, D. W. Thomas and R. Duncan, *J. Controlled Release*, 2008, **130**, 275–283.
21 E. L. Ferguson and R. Duncan, *Biomacromolecules*, 2009, **10**, 1358–1364.
22 R. P. Badman, S. L. Moore, J. L. Killian, T. Feng, T. A. Cleland, F. Hu and M. D. Wang, *Sci. Rep.*, 2020, **10**, 1–14.
23 D. Y. Seo, M. Jin, J. C. Ryu and Y. J. Kim, *J. Toxicol. Environ. Health Sci.*, 2017, **9**, 23–29.
24 H. Sies, C. Berndt and D. P. Jones, *Annu. Rev. Biochem.*, 2017, **86**, 715–748.
25 G. Stark, *J. Membr. Biol.*, 2005, **16**, 1–16.
26 A. Manke, L. Wang and Y. Rojanasakul, *Biomed Res. Int.*, 2013, **2013**, 15.
27 G. C. C. G. Fresta, A. Chakraborty, M. B. Wijesinghe, A. M. Amorini, G. Lazzarino, B. Tavazzi, S. M. Lunte, F. Caraci and P. Dhar, *Cell Death Dis.*, 2018, **9**, 245.
28 S. Pieper and K. Langer, *Mater. Today: Proc.*, 2017, **4**, S188–S192.
29 N. Yeredla, T. Kojima, Y. Yang, S. Takayama and M. Kanapathipillai, *Nat. Publ. Gr.*, 2016, 1–8.
30 C. E. Mora-Huertas, H. Fessi and A. Elaissari, *Int. J. Pharm.*, 2010, **385**, 113–142.
31 S. Khoee and M. Yaghoobian, *Eur. J. Med. Chem.*, 2009, **44**, 2392–2399.
32 E. Castellanos Gil, A. Iraizoz Colarte, J. L. Lara Sampedro and B. Bataille, *Eur. J. Pharm. Biopharm.*, 2008, **69**, 303–311.
33 L. Yang, D. An, T. J. Wang, C. Kan and Y. Jin, *Particuology*, 2017, **30**, 73–82.
34 S. Y. Lin, M. J. Li and K. H. Lin, *AAPS PharmSciTech*, 2004, **5**, 2–6.
35 L. Ma, T. W. Liu, M. A. Wallig, I. T. Dobrucki, L. W. Dobrucki, E. R. Nelson, K. S. Swanson and A. M. Smith, *ACS Nano*, 2016, **10**, 6952–6962.
36 S. Zanganeh, G. Hutter, R. Spitler, O. Lenkov, M. Mahmoudi, A. Shaw, J. S. Pajarinen, H. Nejadnik, S. Goodman, M. Moseley, L. M. Coussens and H. E. Daldrup-link, *Nat. Nanotechnol.*, 2016, **11**, 986–994.
37 Q. Chen, M. Gao, Z. Li, Y. Xiao, X. Bai, K. O. Boakye-Yiadom, X. Xu and X. Q. Zhang, *J. Controlled Release*, 2020, **323**, 179–190.

 This journal is © The Royal Society of Chemistry 2022

Open Access Article. Published on 01 September 2022. Downloaded on 12/29/2025 6:58:32 AM.
This article is licensed under a Creative Commons Attribution 3.0 Unported Licence.

38 Y. S. Kang, J. Y. Kim, S. A. Bruening, M. Pack, A. Charalambous, A. Pritsker, T. M. Moran, J. M. Loeffler, R. M. Steinman and C. G. Park, *Proc. Natl. Acad. Sci. U. S. A.*, 2004, **101**, 215–220.
39 Y. S. Kang, S. Yamazaki, T. Iyoda, M. Pack, S. A. Bruening, J. Y. Kim, K. Takahara, K. Inaba, R. M. Steinman and C. G. Park, *Int. Immunol.*, 2003, **15**, 177–186.
40 H. Unterweger, C. Janko, M. Schwarz, L. Dézsi, R. Urbanics, J. Matuszak, E. Őrfi, T. Fülöp, T. Bäuerle, J. Szebeni, C. Journé, A. R. Boccaccini, C. Alexiou, S. Lyer and I. Cicha, *Int. J. Nanomed.*, 2017, **12**, 5223–5238.
41 M. J. Breiding, *Physiol. Behav.*, 2014, **63**, 1–18.
42 Y. Chao, P. P. Karmali and D. Simberg, Role of Carbohydrate Receptors in the Macrophage Uptake of Dextran-Coated Iron Oxide Nanoparticles, in *Nano-Biotechnology for Biomedical and Diagnostic Research*, Advances in Experimental Medicine and Biology, ed. E. Zahavy, A. Ordentlich, S. Yitzhaki and A. Shafferman, Springer, Dordrecht, 2012, vol. 733, DOI: 10.1007/978-94-007-2555-3_11.
43 S. Józefowski, Z. Yang, J. Marcinkiewicz and L. Kobzik, *Inflammation Res.*, 2012, **61**, 113–126.
44 A. Peigneux, E. A. Glitscher, R. Charbaji, C. Weise, S. Wedepohl, M. Calderón, C. Jimenez-Lopez and S. Hedtrich, *J. Mater. Chem. B*, 2020, **8**, 4870–4882.
45 J. Simon, S. Christmann, V. Mailänder, F. R. Wurm and K. Landfester, *Isr. J. Chem.*, 2018, **58**, 1363–1372.
46 C. D. Walkey, J. B. Olsen, H. Guo, A. Emili and W. C. W. Chan, *J. Am. Chem. Soc.*, 2012, **134**, 2139–2147.
47 G. Caracciolo, D. Pozzi, A. L. Capriotti, C. Cavaliere, S. Piovesana, G. La Barbera, A. Amici and A. Laganà, *J. Mater. Chem. B*, 2014, **2**, 7419–7428.
48 C. Lemarchand, R. Gref, C. Passirani, E. Garcion, B. Petri, R. Müller, D. Costantini and P. Couvreur, *Biomaterials*, 2006, **27**, 108–118.
49 C. Lemarchand, R. Gref and P. Couvreur, *Eur. J. Pharm. Biopharm.*, 2004, **58**, 327–341.
50 K. L. Vigor, P. G. Kyrtatos, S. Minogue, K. T. Al-Jamal, H. Kogelberg, B. Tolner, K. Kostarelos, R. H. Begent, Q. A. Pankhurst, M. F. Lythgoe and K. A. Chester, *Biomaterials*, 2010, **31**, 1307–1315.
51 B. Kang, T. Opatz, K. Landfester and F. R. Wurm, *Chem. Soc. Rev.*, 2015, **44**, 8301–8325.
52 U. Sakulkhu, M. Mahmoudi, L. Maurizi, J. Salaklang and H. Hofmann, *Sci. Rep.*, 2014, **4**, 1–9.
53 V. Mirshafiee, R. Kim, S. Park, M. Mahmoudi and M. L. Kraft, *Biomaterials*, 2016, **75**, 295–304.
54 C. Corbo, R. Molinaro, F. Taraballi, N. E. Toledano Furman, K. A. Hartman, M. B. Sherman, E. De Rosa, D. K. Kirui, F. Salvatore and E. Tasciotti, *ACS Nano*, 2017, **11**, 3262–3273.
55 J. J. Rennick, A. P. R. Johnston and R. G. Parton, *Nat. Nanotechnol.*, 2021, **16**, 266–276.
56 C. Commisso, R. J. Flinn and D. Bar-Sagi, *Nat. Protoc.*, 2014, **9**, 182–192.
57 L. Li, T. Wan, M. Wan, B. Liu, R. Cheng and R. Zhang, *Cell Biol. Int.*, 2015, **39**, 531–539.
58 C. C. Berry, S. Wells, S. Charles, G. Aitchison and A. S. G. Curtis, *Biomaterials*, 2004, **25**, 5405–5413.
59 C. Wilhelm, C. Billotey, J. Roger, J. N. Pons, J. C. Bacri and F. Gazeau, *Biomaterials*, 2003, **24**, 1001–1011.
60 B. S. Joshi and I. S. Zuhorn, *Eur. J. Neurosci.*, 2021, **53**, 706–719.
61 H. C. Christianson and M. Belting, *Matrix Biol.*, 2014, **35**, 51–55.
62 A. Moore, R. Weissleder and A. Bogdanov, *J. Magn. Reson. Imaging*, 1997, **7**, 1140–1145.
63 S. P. Massia, J. Stark and D. S. Letbetter, *Biomaterials*, 2000, **21**, 2253–2261.
64 S. Sritharan and N. Sivalingam, *Life Sci.*, 2021, **278**, 119527.
65 K. E. Coldwell, S. M. Cutts, T. J. Ognibene, P. T. Henderson and D. R. Phillips, *Nucleic Acids Res.*, 2008, **36**, e100.
66 I. Mickuviene, V. Kirveliene and B. Juodka, *Toxicol. In Vitro*, 2004, **18**, 639–648.
67 N. A. Monteiro-Riviere, A. O. Inman and L. W. Zhang, *Toxicol. Appl. Pharmacol.*, 2009, **234**, 222–235.
68 C. B. Assays, C. Cycle, C. Proliferation, C. Death, C. B. Assays, C. Cycle, C. Proliferation, C. D. Like, L. Cobb, L. Angeles, U. States, L. C. S. E. Consulting, L. Angeles, U. S. Doi, M. Methods, S. Buffer, J. B. Gmbh, E. Hervouet, P. F. Cartron, M. Jouvenot, R. Delage-Mourroux, R. Hingorani, J. Deng, J. Elia, C. McIntyre, D. Mittar, G. G. Lin, J. G. Scott, B. Us, P. F. Lambert and S. Chung, *BD Biosci.*, 2016, **8**, 1–2.
69 Ö. S. Aslantürk, *Genotoxicity - A Predict. Risk to Our Actual World*, 2018, pp. 1–18.
70 B. A. Carneiro and W. S. El-Deiry, *Nat. Rev. Clin. Oncol.*, 2020, **17**, 395–417.
71 S. Fulda, *Int. J. Cancer*, 2009, **124**, 511–515.
72 N. C. L. Zembruski, V. Stache, W. E. Haefeli and J. Weiss, *Anal. Biochem.*, 2012, **429**, 79–81.
73 S. Pulakkat, S. A. Balaji, A. Rangarajan and A. M. Raichur, *ACS Appl. Mater. Interfaces*, 2016, **8**, 23437–23449.
74 F. Angius and A. Floris, *Toxicol. In Vitro*, 2015, **29**, 314–319.
75 A. A. Stepanenko and V. V. Dmitrenko, *Gene*, 2015, **574**, 193–203.
76 M. V. D. Z. Park, D. P. K. Lankveld, H. van Loveren and W. H. de Jong, *Nanomedicine*, 2009, **4**, 669–685.
77 S. Wang, H. Yu and J. K. Wickliffe, *Toxicol. In Vitro*, 2011, **25**, 2147–2151.
78 J. M. Wörle-Knirsch, K. Pulskamp and H. F. Krug, *Nano Lett.*, 2006, **6**, 1261–1268.
79 M. Fisichella, H. Dabboue, S. Bhattacharyya, M. L. Saboungi, J. P. Salvetat, T. Hevor and M. Guerin, *Toxicol. In Vitro*, 2009, **23**, 697–703.
80 L. Belyanskaya, P. Manser, P. Spohn, A. Bruinink and P. Wick, *Carbon N. Y.*, 2007, **45**, 2643–2648.
81 A. L. Holder, R. Goth-Goldstein, D. Lucas and C. P. Koshland, *Chem. Res. Toxicol.*, 2012, **25**, 1885–1892.
82 A. J. Gormley and H. Ghandehari, *Evaluation of Toxicity of Nanostructures in Biological Systems*, 2009.
83 A. Kroll, M. H. Pillukat, D. Hahn and J. Schnekenburger, *Arch. Toxicol.*, 2012, **86**, 1123–1136.
84 P. P. Danieli, B. Ronchi and C. Rossi, *Acta Nat. Sci.*, 2014, **1**, 58–61.

85 M. Madesh and K. A. Balasubramanian, *Indian J. Biochem. Biophys.*, 1998, **35**, 184–188.
86 V. C. Soeiro, K. R. T. Melo, M. G. C. F. Alves, M. J. C. Medeiros, M. L. P. M. Grilo, J. Almeida-Lima, D. L. Pontes, L. S. Costa and H. A. O. Rocha, *Int. J. Mol. Sci.*, 2016, **17**, 1–15.
87 M. R. Mohammadi, A. V. Malkovskiy, P. Jothimuthu, K. M. Kim, M. Parekh, M. Inayathullah, Y. Zhuge and J. Rajadas, *Sci. Rep.*, 2018, **8**, 1–11.
88 M. Yu, S. Huang, K. J. Yu and A. M. Clyne, *Int. J. Mol. Sci.*, 2012, **13**, 5554–5570.
89 B. Fadeel and V. E. Kagan, *Redox Rep.*, 2003, **8**, 143–150.

Open Access Article. Published on 01 September 2022. Downloaded on 12/29/2025 6:58:32 AM.
This article is licensed under a Creative Commons Attribution 3.0 Unported Licence.

This journal is © The Royal Society of Chemistry 2022